Dislocations in plastically deformed $L1_2$ compounds based on Al_3Ti

D. G. Morris
Institute of Structural Metallurgy, University of Neuchatel, 2000 Neuchatel, Switzerland

(Received 19 March 1991; accepted 25 September 1991)

The fine structure of dislocations in lightly deformed samples of several cubic ordered alloys with composition based on Al_3Ti has been examined by weak beam electron microscopy. For all the materials examined the dislocations tend to dissociate into two $1/2\langle 110\rangle$ partials separated by APB. Dislocation dissociation is not complete at very small strains and the strain required to dissociate, as well as the dissociation distance, varies from one alloy to another. Improvements in ductility achieved by alloying are directly related to the ease and extent of this dissociation.

I. INTRODUCTION

Trialuminide alloys of titanium are receiving much attention as potential materials for high temperature applications where low density and good oxidation resistance are of critical importance. These materials offer reasonable strength, even up to high temperatures, but are generally extremely brittle. Recent efforts try to understand the underlying causes of this low ductility or toughness and then to improve the overall material properties.

The binary Al_3Ti alloy has the tetragonal $D0_{22}$ structure, is extremely brittle, and deforms at room temperature mostly by twinning.[1] At higher temperatures slip processes start to become important. Two approaches have been attempted to alloy this material and improve ductility: by alloying the $D0_{22}$ material attempting to enhance slip or twin mechanisms,[2] or by alloying to change the crystal structure to the higher symmetry $L1_2$ structure. It is apparently this second approach that is producing the more promising results.

Additions of transition metal elements such as Fe, Cr, and Mn have been shown to produce $L1_2$ ordered materials with reasonable strength and good ductility in compression, both at room temperature as well as at higher temperatures.[3–5] The alloys with Cr and Mn additions have been shown to have a slight ductility when tested in bending,[5] rather than only in compression as for all previous tests. Systematic studies on cubic Al_3Ti based alloys containing such transition metals[6,7] suggest that alloys modified by additions of Cr or Mn are the most ductile, and are the softest of the alloy series examined. Transmission electron microscope examinations show that dislocations may be clearly dissociated after room temperature deformation, in contrast to earlier studies, for example, on Ni modified alloys[8] where no dissociation was apparent, and more distinctly dissociated than on alloys modified with Fe.[9] In recent studies[10,11] of Cr and Mn modified alloys, it is shown that both bend and tensile ductility can be achieved, albeit limited, and that the materials become stronger when tested at low temperatures (down to liquid nitrogen temperature). Similar low temperature strengthening has also been reported for an Fe modified alloy.[12,13] Observations of strengthening at high temperatures have been interpreted in terms of a cube cross slip model, as for Ni_3Al,[10,13,14] a model based on dislocations being dissociated as a pair of $1/2\langle 110\rangle$ partial dislocations separated by APB (anti-phase boundary). The strengthening found at low temperatures is interpreted in terms of a different dissociation,[10,13] as for Pt_3Al, with dislocations dissociated as a pair of $1/3\langle 211\rangle$ separated by CSF (complex stacking fault).

Unreported results[15] show that ductility of the modified Al_3Ti alloys can be correlated with low yield strength and also with low work hardening rate; thus good ductility is associated with easy initial movement of dislocations and with the ability of dislocations to avoid obstacles created during straining. It is clearly important to understand the nature of dislocations within these materials as a function of the test variables: alloy, strain, and temperature. The present report examines the dislocations present within a series of alloys with different ternary element additions, and the variation of dislocation character during the initial straining period.

II. EXPERIMENTAL DETAILS

The materials examined were prepared by spray deposition of prealloyed stock using nitrogen gas for atomization. The deposits obtained, of several kilograms in weight, were subjected to a HIP treatment of 1140 °C for 3 h at 100 MPa in order to remove minor traces of segregation and porosity. Alloy compositions are given in Table I. In addition to the alloys listed here, other alloys containing Fe and Mn + Cr additions have been examined. The alloys chosen are based on earlier work

TABLE I. Compositions (at. %) of alloys studied.

Alloy designation	Aluminum	Titanium	Ternary addition
Al_5Ti_2Cr	67	25	Cr 8
Al_5Ti_2Mn	67	25	Mn 8
Al_5Ti_2Fe	64	28	Fe 8

showing single phase $L1_2$ crystal structures for these compositions.[6,10,16] X-ray diffraction confirmed that the materials were all essentially single phase of $L1_2$ ordered structure. Compression samples 3 mm in diameter and 8 mm long were prepared by spark erosion and tested at a strain rate of 2×10^{-4}/s. For the preparation of the deformed materials examined here samples were deformed only at room temperature to strains of several percent. In view of the possibility of "aging" of the dislocation structures at room temperature,[17] thin foils were prepared and examined as soon as possible after deformation, normally within a few days, or otherwise materials were stored in a refrigerator.

Thin foil samples for transmission electron microscopy were prepared by diamond saw cutting disks from the compression samples, and electrochemically polishing using a twin jet system with a 10% perchloric acid in methanol mixture at −20 °C and 20 V. The thin foils were examined using a Philips CM12 instrument operating at 120 kV using the weak beam mode for fine structure determinations. The contrast condition normally used was about $\mathbf{g}$: 4–5 $\mathbf{g}$. Habit planes of dislocations were determined from the real directions of segments of curved dislocations and confirmed where possible by variations in projected separations of dissociated partials. Bearing in mind that samples examined here were deformed only at room temperature, it is unlikely that climb mechanisms operate and dissociation should thus occur within the slip planes. Separations of partial dislocations were measured directly from micrographs and no corrections for differences between true core separations and image separations were made. The errors introduced in this way are expected to be relatively small, and in particular will not affect comparisons between materials since similar contrast conditions were used throughout the analyses.

III. RESULTS

The present report examines the dislocation structures present after slight deformation of the Al–Ti–Cr, Al–Ti–Mn, and Al–Ti–Fe alloys specified in Table I. It is intended in this way to provide an explanation for the mechanical behaviors of these materials. The mechanical response of the three materials, both at room temperature as well as at elevated temperatures, is presented in detail elsewhere.[15] For the purposes of the present study, the mechanical properties observed at room temperature are summarized in Table II. It is seen that low hardness correlates with low yield stress, low work hardening rate, and higher ductility (in compression as well as in bend testing). The value of the maximum stress at failure in compression depends on both yield stress and failure strain as well as the work hardening rate. Dislocations were examined in samples of each alloy after room temperature deformation to 2%, as well as to 1% and 4% for the Al–Ti–Fe alloy.

Dislocations in the deformed Al–Ti–Fe alloy will be reported first. After deforming only 1% at room temperature, Fig. 1, the dislocations seen are generally smoothly curved and do not show clear signs of any dissociation. Close examination at high magnification shows, however, that some parts of the dislocations are weakly dissociated, as indicated by arrows in Fig. 1. The screw oriented dislocation segments show no sign of dissociation; many segments lie in directions close to 30°, 60°, or 90° from the screw orientation and it is these that show signs of dissociation. Where paired images are seen, one of the images is much weaker than the other, and the general appearance is similar to the double image found from single dislocations when a $\mathbf{g} \cdot \mathbf{b} = 2$ imaging condition is used, even sometimes for weak beam conditions. It is not believed that this is a possible explanation here for the following reasons: many of the dislocations seen in this Al–Ti–Fe alloy do not show double images under the same weak beam conditions used throughout this study (even though in this case the Burgers vector of the single dislocation is clearly $\langle 110 \rangle$ and hence $\mathbf{g} \cdot \mathbf{b} = 2$); second, the image separations observed are typically in the range 3–6 nm when the dislocation habit planes are suitably oriented, and hence much larger than expected for the secondary image artifacts.

TABLE II. Mechanical properties at room temperature.

Alloy designation	Hardness (30 Kg)	Yield stress (MPa)	Maximum stress (MPa)	Failure strain (%)	Work hardening rate (GPa)[a]
Al–Ti–Cr	230	410	1760	23	5.8
Al–Ti–Mn	175	310	1520	24	5.1
Al–Ti–Fe	290	470	1750	19	6.8

[a]Work hardening rate was measured as the stress-strain slope at 5% strain estimated over a 1% strain range.

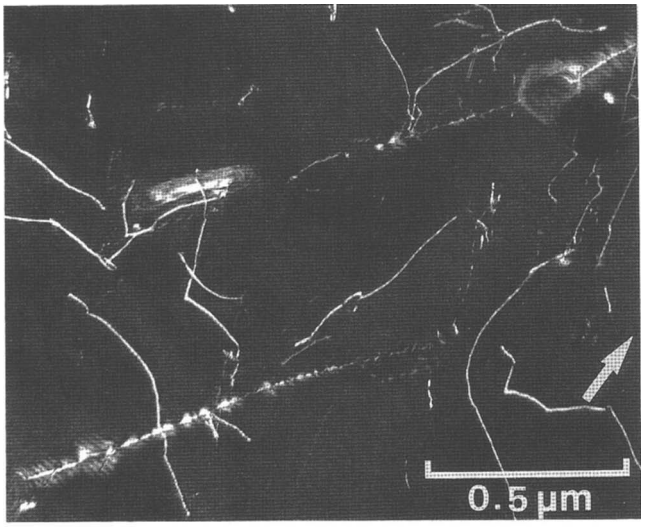

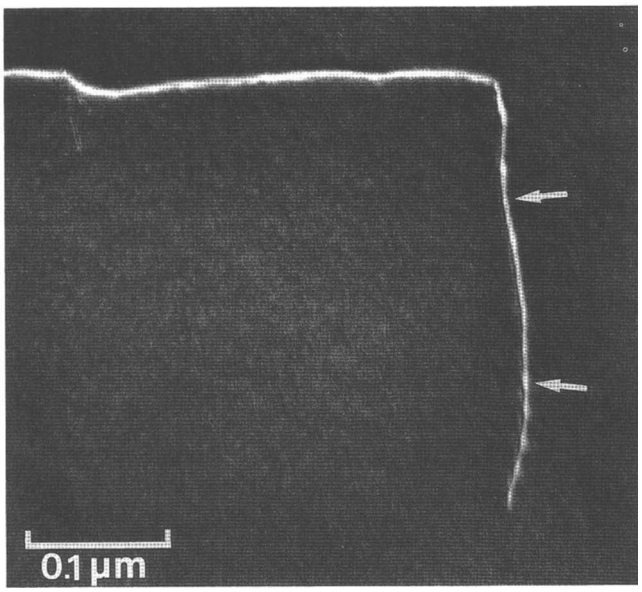

FIG. 1. Dislocations in Al–Ti–Fe deformed 1% at room temperature. Weak beam micrographs; foil orientation (101), diffraction vector, shown, $\bar{1}\,\bar{1}1$. Some of the edge component dislocations are weakly dissociated.

Deformation to 2% for the Al–Ti–Fe alloy leads to little change, and the dislocations still show only faint indications of localized dissociation. Straining to 4% leads to virtually the complete dissociation of all the dislocations seen, Fig. 2. The dissociation distance varies greatly from one segment to another (more than a factor of four), even for segments having about the same edge or screw character. This may be because some parts of the dislocation dissociate earlier than other parts, or dissociation may start at certain preferential points. The fact that the dislocation does not subsequently smoothen to a uniform dissociation distance suggests that large lattice frictional forces may act on the dislocations. (This variability in dissociation distance is not caused

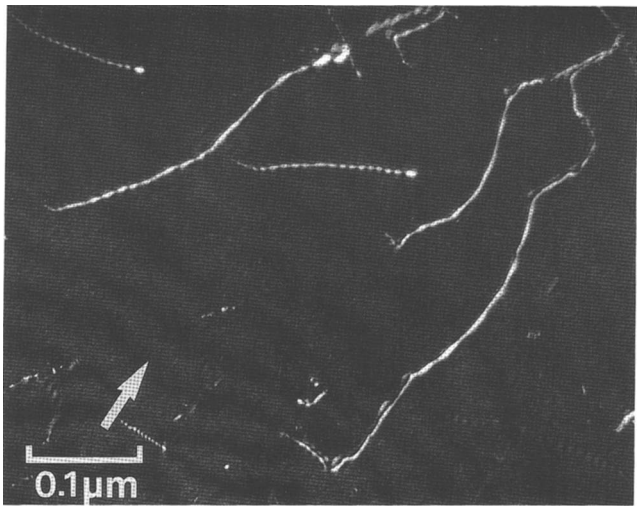

FIG. 2. Al–Ti–Fe deformed 4% at room temperature. Foil orientation (011), diffraction vector $1\bar{1}1$.

by a change in habit plane of the dislocations, as discussed later.) The observation that dislocations are most frequently found lying in specific directions (near screw, 30°, 60°, or 90°) supports this suggestion that friction forces are significant and that the dislocations are lying near specific Peierls valleys.

Figure 3 examines in detail some edge dislocations in the Al–Ti–Fe alloy deformed 2%. The dislocation segments shown are clearly dissociated over projected distances of 2–3 nm. Imaging these dislocations under various diffraction conditions and orientations allows identification of the Burgers vectors of the partial dislocations: dislocation "a" is dissociated into two partial dislocations each with Burgers vector parallel to $[\bar{1}10]$, dislocation "b" to [101], and dislocation "c" to [101]. The identification procedure is exemplified by the invisibility (of both partials in each case) of "b" and "c" when using a 020 **g** vector, and dislocation "a" with the 002 **g** vector. Such invisibility is possible only when dissociation into two partials of type $1/2\langle 110\rangle$ occurs and not possible when dissociation into partials of type $1/3\langle 211\rangle$ occurs. Figures 3(f) and 3(g) show dislocations "a" and "b" under the same imaging conditions as for Figs. 3(a) and 3(b), at a higher magnification, showing clearly the visibility or invisibility of both partial dislocations, according to the dislocation and imaging condition. It should be noted that the dislocations are never totally invisible for any **g** vector in weak beam here, and this is due to the sensitivity of the weak beam contrast mode to elastic anisotropy of the present material and to the fact that the $\mathbf{g} \cdot \mathbf{b} \wedge \mathbf{u} = 0$ condition is not achieved, where **u** is the dislocation line direction. Examination of the projected dislocation dissociation distance as a function of orientation of the sample under study confirms that the habit plane is always of type {111}: for example, dislocation "b" is clearly dissociated at 110, 010, and

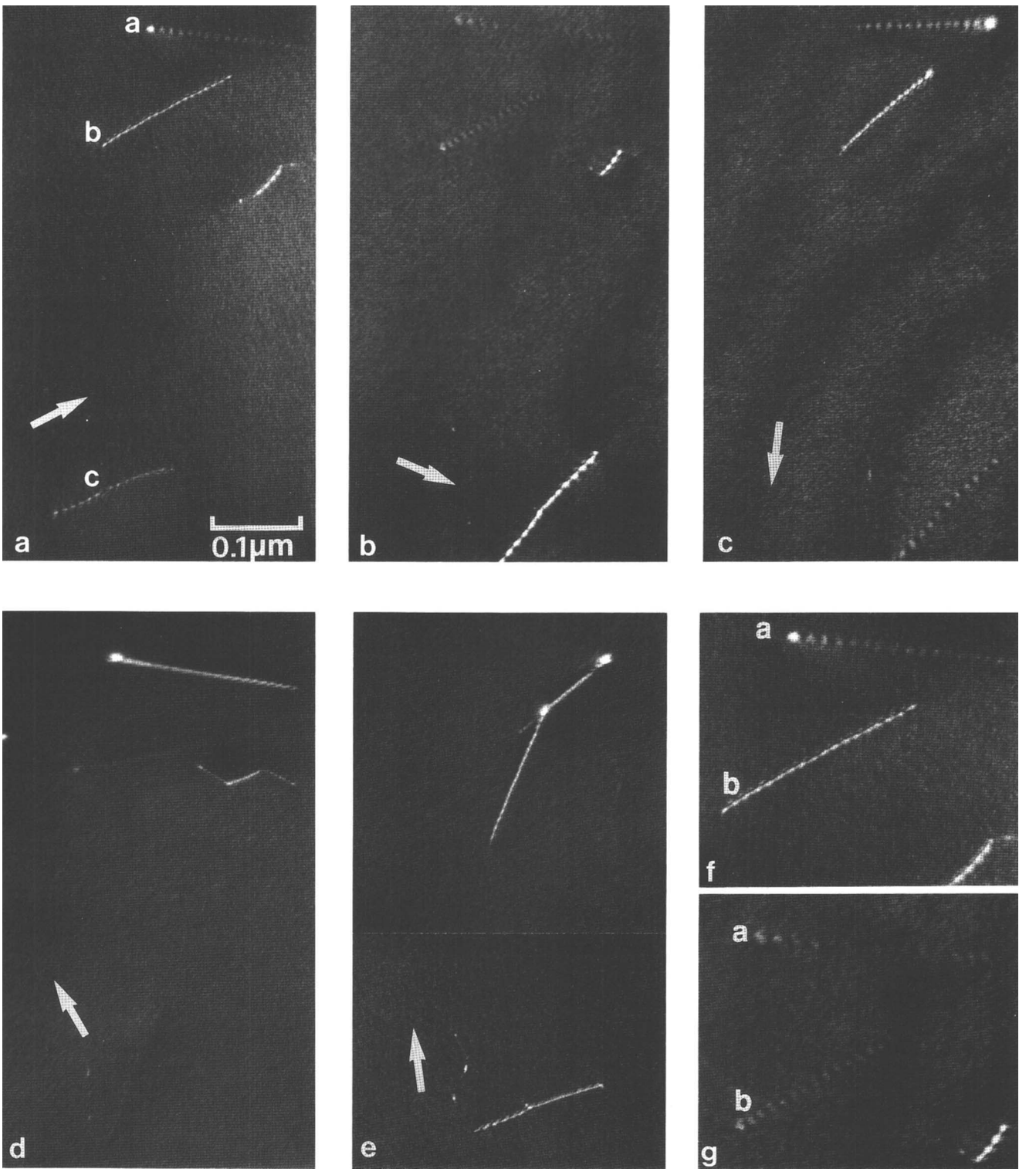

FIG. 3. Al–Ti–Fe deformed 2% at room temperature illustrating Burgers vector analysis and habit plane determination. (a) Foil orientation (110), diffraction vector 002; (b) foil orientation (110), diffraction vector $\bar{1}11$; (c) foil orientation (110), diffraction vector $1\bar{1}1$; (d) foil orientation (100), diffraction vector 020; (e) foil orientation (010), diffraction vector 200; (f) same conditions as (a), at higher magnification; (g) same conditions as (b), at higher magnification.

100 orientations and is apparently much less dissociated near the 011 orientation (not shown)—hence the habit plane of dissociation is $(\bar{1}\,\bar{1}1)$.

The appearance of these paired dislocations is characterized by a stronger contrast for one of the partials than for the other. This may lead to a possible mis-

interpretation as two partial dislocations of different Burgers vector (direction or magnitude). This possibility is eliminated in Fig. 4, which shows the two dislocations "a" and "b" of Fig. 3 when imaged under weak beam conditions using $+\mathbf{g}$ and $-\mathbf{g}$ vectors, where it is seen that the weaker intensity partial is determined by the contrast conditions and not by the dislocation itself. This pair of micrographs confirms also that the paired dislocation seen is a superdislocation and not a dipole, since there is no change in separation of the two lines. It should also be noted that superdislocation "a" seen in Fig. 4 is "invisible" and is distinguished only in residual contrast.

Figure 5 gives another view of the dislocations "a" and "b" (from Figs. 3 and 4) where the thickness fringes are seen to be disturbed by the presence of the dislocations. It is known that the presence of dislocations leads to the formation of additional thickness fringes around a dislocation and the number of fringes is equal to the

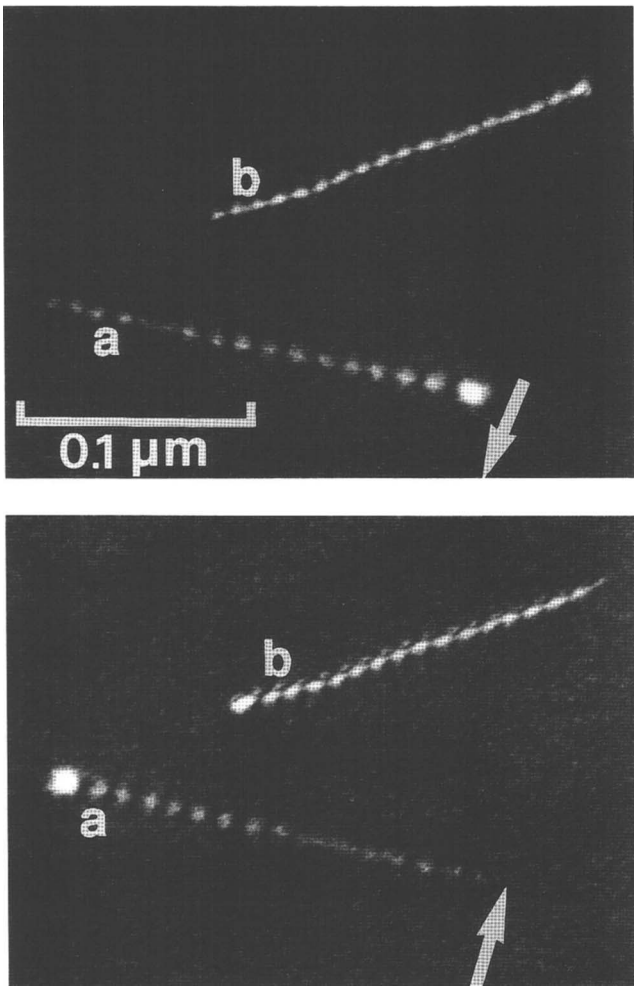

FIG. 4. Al–Ti–Fe deformed 2% at room temperature. Weak beam micrographs taken using $+\mathbf{g}$ and $-\mathbf{g}$ contrast conditions. Foil orientation (110), diffraction vector $1\bar{1}1$. The dislocations shown are the same "a" and "b" as shown in Fig. 3.

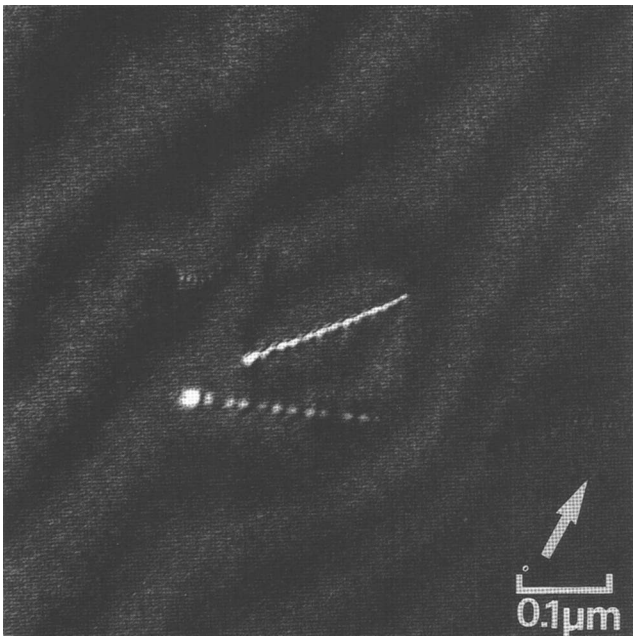

FIG. 5. Al–Ti–Fe deformed 2% at room temperature showing thickness fringes on dislocations. Foil orientation $(21\bar{1})$, diffraction vector $1\bar{1}1$. Dislocation "a" is nominally invisible and has no extra thickness fringes; for dislocation "b" $\mathbf{g} \cdot \mathbf{b} = 2$ and two thickness fringes are tied to each end of the dislocation. The dislocations are the same two as shown in Fig. 4.

product $\mathbf{g} \cdot \mathbf{b}$.[18] In the case of dislocation "a" here there are no new fringes tied to the ends of the dislocation, thus confirming that $\mathbf{g} \cdot \mathbf{b} = 0$ ($\mathbf{g}$ here is $1\bar{1}1$ and $\mathbf{b}$ total is [110]); the dislocation is seen only in residual contrast. Dislocation "b" has two additional thickness fringes attached to each end of the dislocation; both fringes leave one end of the dislocation to join the other end. This observation is confirmation that $\mathbf{g} \cdot \mathbf{b} = 2$; that is, the total Burgers vector of the dislocation is [101], and this is again confirmed to be a superdislocation and not a dipole or other pair of dislocations.

Figure 6 shows a straight dislocation in the Al–Ti–Fe alloy deformed 1% at room temperature and stored for 6 months (at room temperature) before observation. The dislocation shown is near screw orientation, yet shows clear signs of dissociation, at least at some locations. The dislocation has a total Burgers vector of $[0\bar{1}1]$ and is nominally invisible in Fig. 6(b) using a 200 $\mathbf{g}$ vector for imaging. It may be noticed that when the dislocation is clearly dissociated, as from point 3 to 4, and from 5 to 6, the residual contrast in Fig. 6(b) is strongest, and when the dislocation is not dissociated, as for example from point 1 to 2, the residual contrast is very weak; this may suggest that it is the APB fault that is in some way responsible for the residual contrast seen, even though $\mathbf{g} \cdot \mathbf{R}$ for the fault is supposedly zero. It is clear that superlattice beams such as 100 will also be

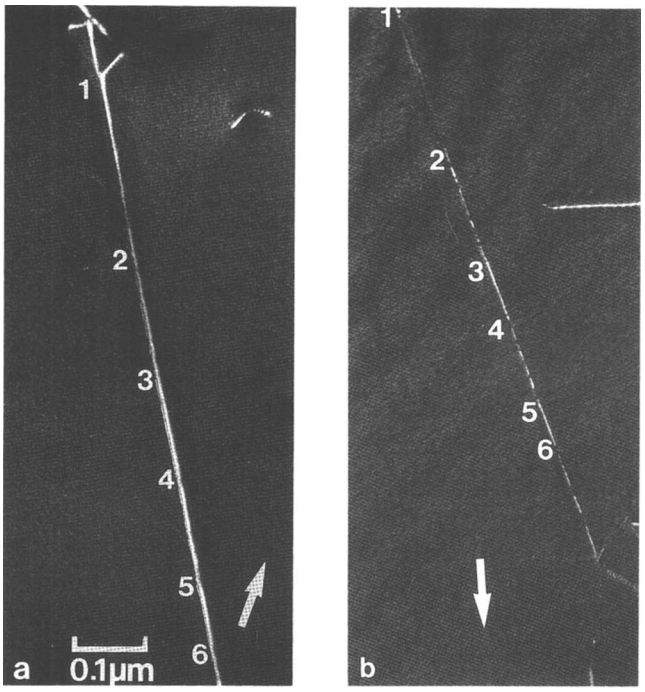

FIG. 6. Al–Ti–Fe deformed 1% at room temperature and stored 6 months at room temperature before examination. (a) Foil orientation $(\bar{1}21)$, diffraction vector 202; (b) foil orientation (010), diffraction vector 200. Superdislocation dissociation is clear between points 3 and 4 and between points 5 and 6.

excited along the 200 systematic row, and hence the APB contrast observed will be associated with interaction amongst these beams. However, a better understanding of the nature of the dislocation cores would require image simulation experiments. Based on the projected spacings when the superdislocation is imaged under different orientations, it appears that the dislocation is dissociated on the $(\bar{1}11)$ plane. It has previously been mentioned, when discussing Figs. 1 and 2, that the extent and distance of dissociation is somewhat variable from one dislocation to another. However, the dislocation shown in Fig. 6 appears to be more dissociated (after 6 months at room temperature) than for the freshly deformed materials, an effect similar to the aging of dislocations seen when heating at moderate temperatures, e.g., 300 °C.[17]

Figure 7 shows dislocations in the Al–Ti–Fe alloy after deforming at room temperature to 4%, where the dissociation is more clear for a larger range of dislocation orientations and over greater segment lengths, and hence the identification of dissociated dislocations and their Burgers vectors is easier. Two dislocations are marked, both with total Burgers vector [011], and dissociated into superdislocations with each partial of Burgers vector 1/2[011]. This is clearly demonstrated by the invisibility when using the 200 and $1\bar{1}1$ **g** vectors. The more straight dislocation is an edge dislocation of 60° character, and the habit plane of the APB is $(\bar{1}\,\bar{1}1)$.

A few tests were carried out at low temperature on this Al–Ti–Fe alloy by cooling the compression sample and platens to liquid nitrogen temperature. The behavior was essentially that seen at room temperature as far as it was possible to judge, namely a yield stress of 495 MPa and similar initial work hardening rate. The system used did not allow deformation in excess of about 5%. Dislocations were examined after deforming about 2% in this way, and no difference between this and room-temperature-deformed samples was seen. Dislocations were mostly in 30°, 60°, and 90° edge orientations and were weakly dissociated to the same 2–3 nm separation; partial dislocations were $1/2\langle 110\rangle$.

After testing at any elevated temperature the dislocations seen were all totally dissociated, as illustrated in Fig. 8 for a sample deformed 4% at 300 °C. The dissociation distance, about 5 nm, is also considerably larger than seen after room temperature deformation. As discussed elsewhere,[15] over the temperature range from room temperature to 300 °C the mechanical properties hardly change, and the dislocations are dissociated as superdislocations with APB between the partials after such higher temperature deformation.

Figure 9 shows dislocations within the Al–Ti–Mn alloy after deforming 2% at room temperature. The dislocations seen here should be compared with those of the Al–Ti–Fe alloy shown in Figs. 1, 2, and 3. The dislocations in the Al–Ti–Mn alloy are more obviously dissociated than those of the Al–Ti–Fe alloy after deforming to 1 or 2% strain, perhaps because the dissociation distance of the partial dislocations is somewhat greater. These dislocations are again mostly of 30°, 60°, or 90° character, and dissociation takes place to a pair of $1/2\langle 110\rangle$ dislocation partials separated by APB lying on the {111} plane. Figure 10 shows dislocations within the Al–Ti–Cr alloy, also after deforming 2% at room temperature. The dislocations seen are similar to those of the Al–Ti–Mn alloy, namely clearly dissociated on the {111} plane.

Figure 11 shows the dissociation distance of the superdislocations after room temperature deformation of the three alloys. Comparison is made for materials deformed 2%, as well as for the Al–Ti–Fe alloy deformed 4% at room temperature. The dislocations seen in the Al–Ti–Fe alloy are somewhat less separated after 2% deformation than the dislocations in the Al–Ti–Mn and Al–Ti–Cr alloys, which have essentially the same separation of the partial dislocations. Deformation of the Al–Ti–Fe alloy to 4% deformation leads to a wider dispersion in dislocation spacings, as shown in Fig. 2, and indicated in Fig. 11 by the large error bars. The influence of such additional straining may be to pin some of the dislocations in excessively large dissociation

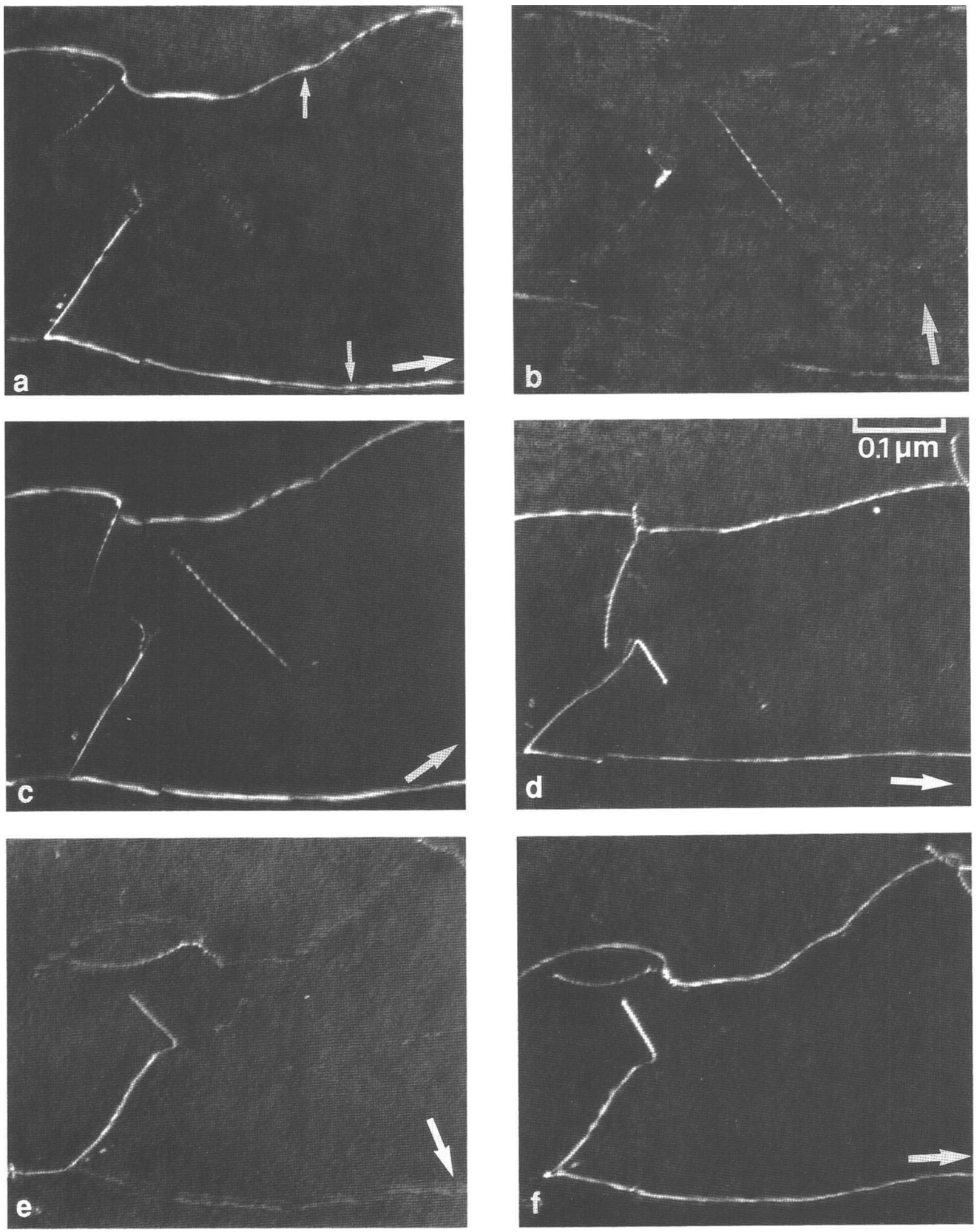

FIG. 7. Al–Ti–Fe deformed 4% at room temperature. Micrographs illustrate Burgers vector analysis and dissociation habit plane identification. (a–c) Foil orientation (110) and diffraction vectors $\bar{1}11$, $1\bar{1}1$, and 002; (d) foil orientation (101), diffraction vector $\bar{1}11$; (e) foil orientation $(02\bar{1})$, diffraction vector 200; (f) foil orientation $(01\bar{1})$, diffraction vector $\bar{1}11$.

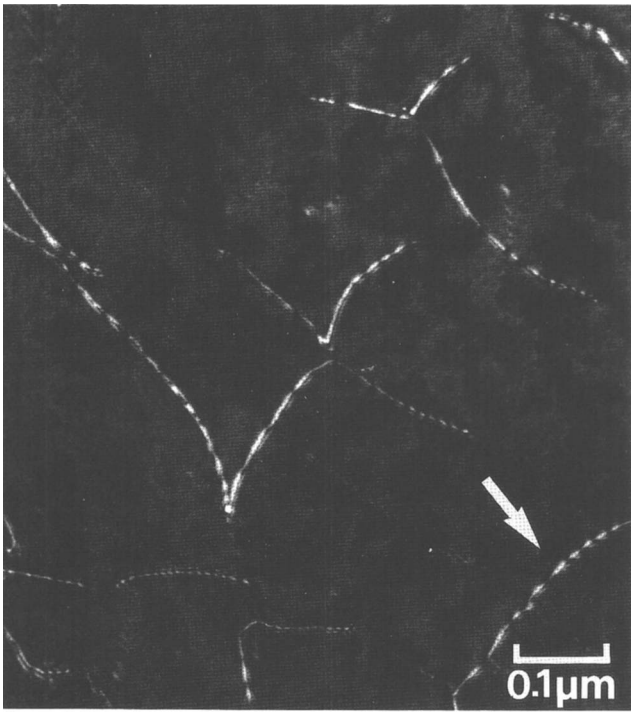

FIG. 8. Al–Ti–Fe deformed 4% at 300 °C. Foil orientation (110), diffraction vector $\bar{1}11$.

configurations under the influence of local internal stress variations or friction forces.

IV. DISCUSSION

The present study has examined the mechanical behavior of a series of Al–Ti–X alloys all essentially single phase, having the $L1_2$ crystal structure, and with a chemical formula which can be expressed schematically as Al_5XTi_2. The alloys examined have been selected based on previous work which has shown that the choice of X as Fe, Mn, or Cr can lead to materials having reasonable strength and showing traces of ductility when tested in bending or in tension. In the present case compression tests have been reported and it has been shown that improvements in ductility can be correlated with lower yield stress and hardness and with lower work hardening rates (Table II). The alloy containing Fe is the hardest, has the highest work hardening rate, and is the most brittle, both in compression as well as in bending. The alloys containing Cr and Mn are more similar in properties, with the Mn alloy being slightly softer, of lower work hardening rate, and more ductile.

It should be pointed out at this stage that the materials studied did contain small amounts of second phase particles; see, for example, Refs. 14 and 15. The second phases were identified as mostly Al_2Ti, based both on EDS and electron diffraction analysis. The second phase particles were typically present as transgranular blocky

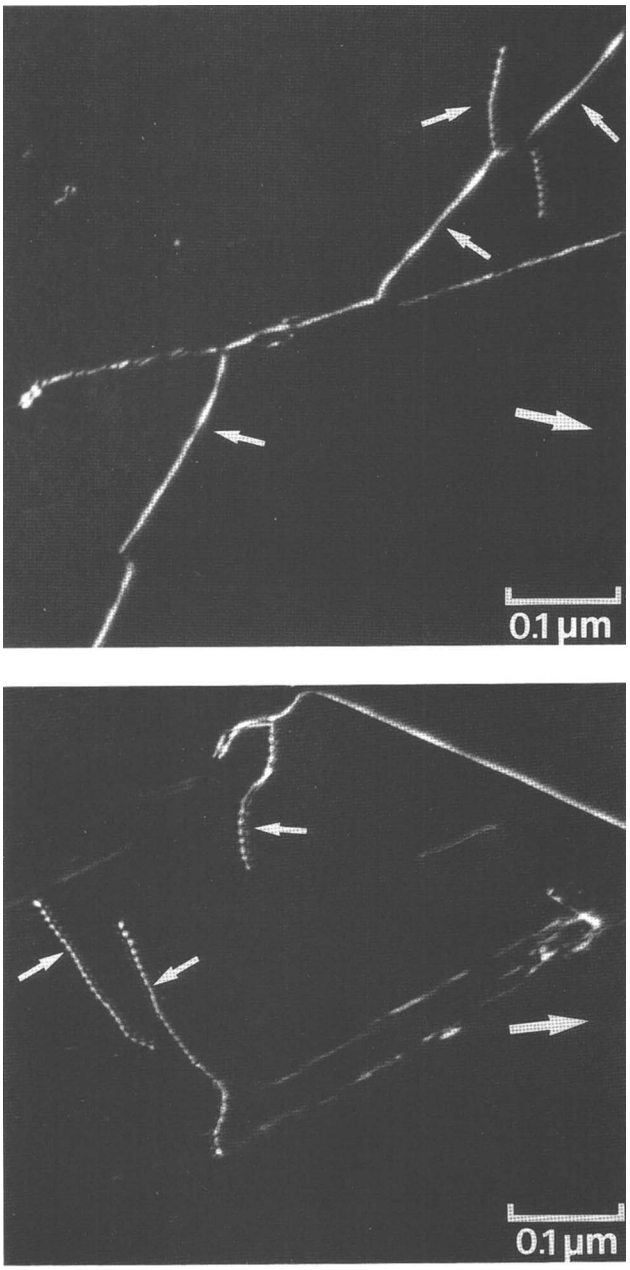

FIG. 9. Two examples of dislocations in Al–Ti–Mn deformed 2% at room temperature. Foil orientation (110), diffraction vector $1\bar{1}1$.

particles of size about $1/4$ to $1/2$ μm, and were present in a volume fraction well below 1%. These particles may play a minor role in modifying either strength or ductility, but it is not believed that their influence was a major one.

The work here of examining dislocation configurations shows that the dislocations always dissociate into a pair of $1/2\langle 110\rangle$ partial dislocations, separated by an APB lying on the $\{111\}$ plane. The dissociation distance, summarized in Fig. 11, is seen to be generally smaller for the Fe containing alloy after comparative

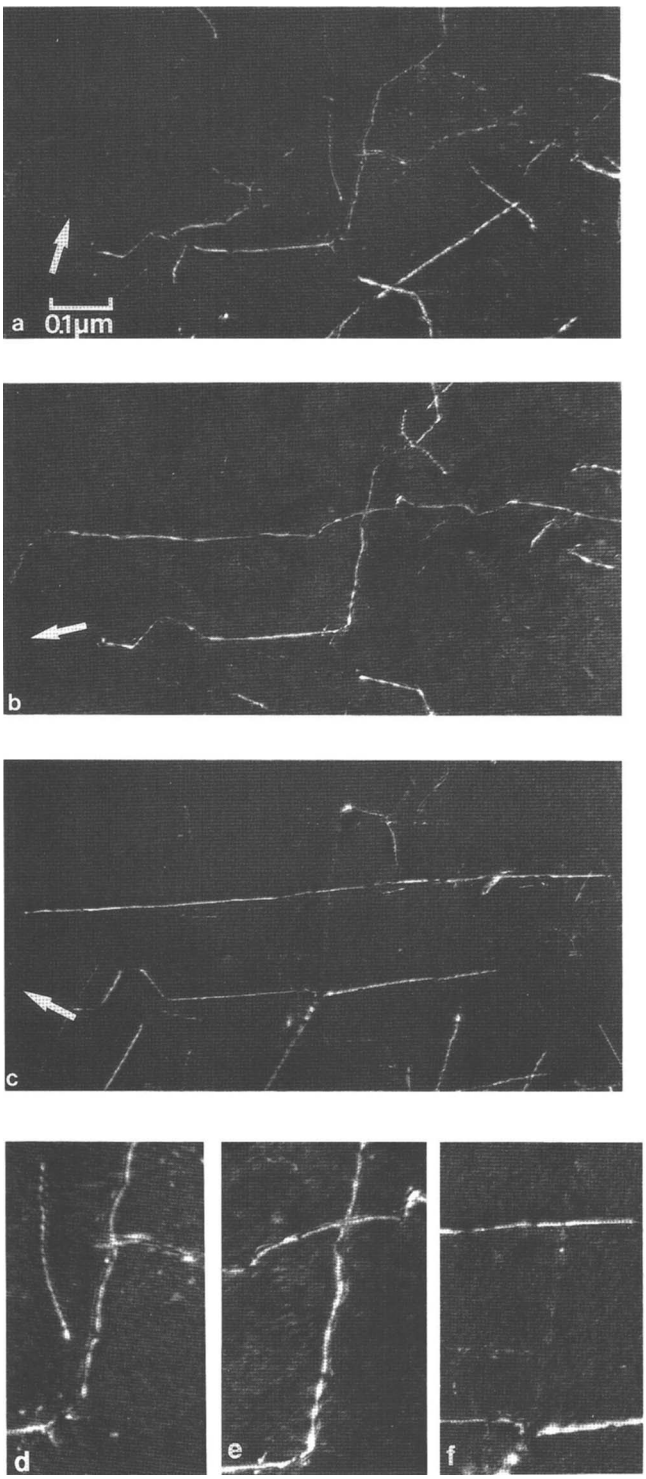

FIG. 10. Al–Ti–Cr deformed 2% at room temperature. (a) Foil orientation (011), diffraction vector 200; (b) foil orientation (011), diffraction vector $1\bar{1}1$; (c) foil orientation (110), diffraction vector 002. (d), (e), and (f) are higher magnification micrographs showing the central parts of (a), (b), and (c).

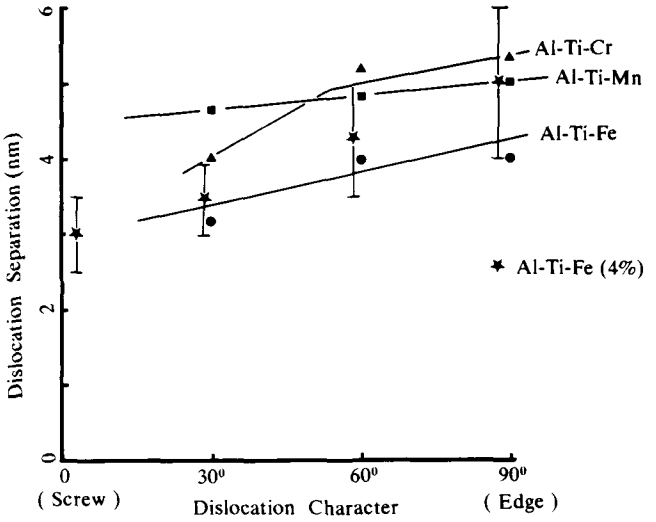

FIG. 11. Dislocation dissociation distances in the Al–Ti–Fe, Al–Ti–Mn, and Al–Ti–Cr materials deformed 2% (also 4% for the Al–Ti–Fe) as a function of dislocation character, θ, the angle between Burgers vector and line direction.

amounts of strain (2%). The Al–Ti–Mn and Al–Ti–Cr alloys have similar dissociation distances, and it is not possible, in view of the dispersion of experimental measurements, to distinguish between these two alloys. The Al–Ti–Fe alloy is characterized both by a slightly smaller dissociation distance as well as a greater difficulty in achieving dissociation: after 1–2% strain the Al–Ti–Fe alloy contains dislocations that are mostly undissociated, and 4% strain is required to dissociate essentially all the dislocations; after 2% strain, the Al–Ti–Mn and Al–Ti–Cr alloys contain dislocations that are mostly dissociated already, to the wider separation characterizing these materials. It can be concluded that the Al–Ti–Mn and Al–Ti–Cr lattices are more suitable for dislocation dissociation into superdislocations separated by APB, and that this is responsible for a lower yield stress, easier dislocation movement, and lower work hardening rate; also, less dislocation debris is produced by deformation and continued dislocation motion remains easy. The consequence is, finally, an enhanced ductility of the material.

The observation of dislocation dissociation which depends on the amount of strain is unusual and is not completely understood. A possible explanation is that the dissociation process may depend on stress or time, as would be expected for a thermally activated process. Similarly, the observation of thermally induced relaxation of the APB separating the two partial dislocations, even at low temperatures (e.g., 300 °C) in very short times,[17] may indicate that relaxation occurring after straining or after unloading may play a role. The influence of such test parameters on dislocation structures is the subject of future work.

Dissociation of the dislocations in this way leaves open the possibility for cross slip to cube planes at higher temperatures, provided the APB energy anisotropy or

elastic anisotropy is suitable. Such cube cross slip may then explain, at least in principle,[14] the stress increases observed when testing at high temperatures. The observation of the same dissociation (two $1/2\langle 110\rangle$ partial dislocations separated by APB on the $\{111\}$ plane) even after testing at low temperatures is consistent with the observation here of no exceptional strengthening at the low temperature. These low temperature results (mechanical data) are in marked disagreement with other published work[10,12,13] which show significant increases in strength on testing at low temperature. Dislocation analysis on these materials has not been reported. It appears that the family of Al–Ti–X alloys may be sensitive to slight variations in alloy composition, or in impurity content, and variable results may be found at low temperature, just as seen before at higher temperatures—for example, Ref. 10. In other (unpublished) studies it has been found that repeat casts or spray deposits of nominally identical compositions (showing slight differences in chemical composition) can have widely differing mechanical properties near certain composition ranges; in the case of the Al–Ti–Fe alloys studied this variability has been seen to coincide with the appearance of second phases. Results similar to this have also been reported by DiPietro *et al.*,[19] who showed that small changes in chemical composition of similar Al–Ti–Fe alloys led to the formation of various second phases, presumably by precipitation, and hence that the single phase region of the $L1_2$ phase was of very limited extent.

Finally, it is interesting to speculate on the reasons for the differences in behavior of the Fe, Mn, and Cr containing alloys. It seems likely that the improved ductility observed is due to the easier formation of $1/2\langle 110\rangle\{111\}$ faults, as found between the more-readily dissociated dislocations. It has been suggested that the addition of Mn or Cr may be beneficial to softening the Al_3Ti alloy through more effective destabilization of the $D0_{22}$ structure and the replacement of Al_p–Ti_d electron bonds by Ti_d–M_d bonds.[6] At the same time the total effective bond strength is changed,[6] as reflected in the increasing lattice parameter of the $L1_2$ phase when substitution occurs using the elements Cr or Mn. In a similar way, for the TiAl phase,[20] it has been shown that substitution of Al by M to enhance the Ti_d–M_d bonds and to maintain weak the Al_p–M_d bonds should enhance ductility, and furthermore that this should be better achieved by substituting Al by elements such as Cr or Mn, rather than by elements such as Fe. It is not possible to decide here whether the improvements seen are the result of changes in bond character, as proposed by Morinaga *et al.*[20] for TiAl, or changes in the total effective bond strength, as suggested by the results of Nic *et al.*[6]

ACKNOWLEDGMENTS

The author is grateful to G. Hollrigl of Alusuisse-Lonza for the preparation of materials and to R. Lerf for the mechanical testing. This work was supported in part by the Swiss Commission for the Encouragement of Scientific Research and in part by the Swiss National Science Foundation.

REFERENCES

1. M. Yamaguchi, Y. Umakoshi, and T. Yamane, Philos. Mag. A **55**, 301 (1987).
2. M. Yamaguchi, Y. Umakoshi, and T. Yamane, in *High-Temperature Ordered Intermetallic Alloys II,* edited by N. S. Stoloff, C. C. Koch, C. T. Liu, and O. Izumi (Mater. Res. Soc. Symp. Proc. **81**, Pittsburgh, PA, 1987), p. 275.
3. K. S. Kumar and J. R. Pickens, Scripta Metall. **22**, 1015 (1988).
4. H. Mabuchi, K. Hirukawa, and Y. Nakayama, Scripta Metall. **23**, 1761 (1989).
5. S. Zhang, J. P. Nic, and D. E. Mikkola, Scripta Metall. **24**, 57 (1990).
6. J. P. Nic, S. Zhang, and D. E. Mikkola, Scripta Metall. **24**, 1099 (1990).
7. S. Zhang, J. P. Nic, W. W. Milligan, and D. E. Mikkola, Scripta Metall. **24**, 1441 (1990).
8. C. D. Turner, W. O. Powers, and J. A. Wert, Acta Metall. **37**, 2635 (1989).
9. E. P. George, J. A. Horton, W. D. Porter, and J. H. Schneibel, J. Mater. Res. **5**, 1639 (1990).
10. S. A. Brown, K. S. Kumar, and J. D. Whittenberger, Scripta Metall. et Mater. **24**, 2001 (1990).
11. K. S. Kumar, S. A. Brown, and J. D. Whittenberger, in *High Temperature Ordered Intermetallic Alloys IV,* edited by L. A. Johnson, D. P. Pope, and J. O. Stiegler (Mater. Res. Soc. Symp. Proc. **213**, Pittsburgh, PA, 1991), p. 481.
12. Z. L. Wu, D. P. Pope, and V. Vitek, Scripta Metall. et Mater. **24**, 2187 (1990).
13. Z. L. Wu, D. P. Pope, and V. Vitek, Scripta Metall. et Mater. **24**, 2191 (1990).
14. D. G. Morris and R. Lerf, in *High Temperature Ordered Intermetallic Alloys IV,* edited by L. A. Johnson, D. P. Pope, and J. O. Stiegler (Mater. Res. Soc. Symp. Proc. **213**, Pittsburgh, PA, 1991), p. 305.
15. R. Lerf and D. G. Morris, to be published.
16. S. Mazdiyasni, D. B. Miracle, D. M. Dimiduk, M. G. Mendiratta, and P. R. Subramanian, Scripta Metall. **23**, 327 (1989).
17. D. G. Morris, Philos. Mag. (in press).
18. M. H. Loretto, in *Electron Beam Analysis of Materials* (Chapman and Hall, London, 1984), p. 124.
19. M. S. DiPietro, K. S. Kumar, and J. D. Whittenberger, J. Mater. Res. **6**, 530 (1991).
20. M. Morinaga, J. Saito, N. Yukawa, and H. Adachi, Acta Metall. et Mater. **38**, 25 (1990).